




## Tracing engineered nanomaterials in biological tissues using coherent anti-Stokes Raman scattering (CARS) microscopy – A critical review

Rhys M. Goodhead, Julian Moger, Tamara S. Galloway & Charles R. Tyler


To cite this article: Rhys M. Goodhead, Julian Moger, Tamara S. Galloway & Charles R. Tyler (2015) Tracing engineered nanomaterials in biological tissues using coherent anti-Stokes Raman scattering (CARS) microscopy – A critical review, *Nanotoxicology*, 9:7, 928-939, DOI: [10.3109/17435390.2014.991773](https://doi.org/10.3109/17435390.2014.991773)

To link to this article: <https://doi.org/10.3109/17435390.2014.991773>

 View supplementary material 

 Published online: 11 May 2015.

 Submit your article to this journal 

 Article views: 609

 View related articles 

 View Crossmark data 

 Citing articles: 6 View citing articles 

REVIEW ARTICLE

## Tracing engineered nanomaterials in biological tissues using coherent anti-Stokes Raman scattering (CARS) microscopy – A critical review

Rhys M. Goodhead<sup>1,2</sup>, Julian Moger<sup>2</sup>, Tamara S. Galloway<sup>1</sup>, and Charles R. Tyler<sup>1</sup>

<sup>1</sup>Environment and Evolution Research Group, College of Life and Environmental Sciences, University of Exeter, Exeter, UK and <sup>2</sup>School of Physics, University of Exeter, Exeter, UK

### Abstract

Nanomaterials (NMs) are used in an extremely diverse range of products and are increasingly entering the environment, driving a need to better understand their potential health effects in both humans and wildlife. A major challenge in nanoparticle (eco)toxicology is the ability to localise NMs post exposure, to enable more targeted biological effects analyses. A range of imaging techniques have been applied to do so, but they are limited, requiring either extensive processing of the material, staining or use of high intensity illumination that can lead to photo damage and/or have limited tissue penetration. Coherent anti-Stokes Raman scattering (CARS) microscopy is a label-free imaging technique, providing contrast based on the intrinsic molecular vibrations of a specimen, circumventing the need for chemical perturbation by exogenous labels. CARS uses near infra-red excitation wavelengths which allow microscopy at depths of several hundred microns in intact tissues and minimises photo-damage to live and delicate samples. Here we provide an overview of the CARS process and present a series of illustrative examples demonstrating its application for detecting NMs within biological tissues, ranging from isolated cells to whole organisms and including materials spanning metals to polymers. We highlight the advantages of this technique which include chemically selective live imaging and substantial depth penetration, but we also discuss its limitations when applied to nanotoxicology, which most notably include the lack of resolution for studies on single nanoparticles.

### Keywords

Biodistribution, imaging, nanotoxicology, non-linear, uptake

### History

Received 22 July 2014  
Revised 20 November 2014  
Accepted 20 November 2014  
Published online 11 May 2015

### Introduction

The potential health effects associated with exposure to nanomaterials (NMs) are now of major international concern. With the rapid expansion in NM applications (global sales topping €450 billion in 2010; Grieger et al., 2010), precautionary approaches have been called for until the desirable properties these materials offer to medicine and industrial applications are better defined in terms of their potential health risks (Oberdorster, 2010). As a consequence, there are extensive research programmes internationally to investigate the potential hazards associated with exposure to NMs. Exposure studies have been conducted in many organisms and systems, however, most have been acute in nature and at regimes that far exceed the levels of NMs present (or predicted) in almost all compartments of the environment. Findings from these studies have also been variable and often lack consensus for any one NM. For some NMs such as silver (Ag) there appears to be cause for concern (Schrand et al., 2010) whereas for others, the predominant data would suggest may be less concern (e.g. titanium dioxide, TiO<sub>2</sub>, reviewed in

Menard et al., 2011). Even for TiO<sub>2</sub> as a NM, however, a recent study suggests that this material may induce oxidative stress in fish when exposed in the presence of ultra-violet light (Bar-Ilan et al., 2013). It should be recognised that there are extremely few studies that have considered chronic health effects and relatively few NMs have been tested thoroughly, or in any standardised manner. Many of the reported eco(toxicology) studies have provided limited information on the associated NM characteristics within the exposure system and this in turn has made it difficult to draw comparisons across studies and to establish, with precision, the nature of the exposure material. Among the plethora of emerging exposure data, even less attention has been directed towards establishing the target sites for NM in the exposed animals, and this is fundamental for advancing our understanding on what the (likely) associated health outcome(s) might be. An exception to this is for airborne exposures to selected NMs (e.g. carbon nanotubes), some of the earliest particles studied (Tantra & Cumpson, 2007), which can contribute to pulmonary diseases, inflammation and fibrosis, including by novel mechanisms (reviewed in Lam et al., 2006).

There are a number of techniques that have been applied to quantify and visualise NM uptake in biological systems and a brief overview on these and their advantages and disadvantages are given in Table 1. These methods have included inductively coupled plasma mass spectroscopy (ICP-MS) and single

Table 1. Advantages and disadvantages of common techniques used to quantify and localise NMs within biological samples.

Technique	Advantages	Disadvantages
ICP-MS Electron microscopy	Excellent quantification. Very high imaging resolution.	Poor localisation ability. Terminal sampling of the organism and extensive sample preparation are required. Quantification tedious and analysis practically confined to part of the tissue or cell.
Dark-field single optical microscopy Confocal microscopy	Real time imaging with nanometre resolution. Ability to count individual particles. Thin optical sectioning capabilities. Quantification is possible, but limited to certain probes (e.g. fluorescence) which is an indirect measurement.	High intensity illumination can lead to photodamage. Minimal tissue penetration. Sample needs modification by contrast agent. Low spatial resolution.
CARS microscopy	Label free, IR wavelengths reduce photodamage and allow deep tissue penetration. Provides complementary chemical information.	~200 nm resolution. Information derived is not easily quantified.

nanoparticle (SN ICP-MS) on tissue extracts (Ferry et al., 2009; Scown et al., 2009), the use of radioactively labelled NMs to trace NM transport and tissue localisation (Lu et al., 2010; Sumner et al., 2010), and more recently, stable isotope tracing for the detection of metal based NMs in samples with high natural background levels of the respective elements (Larner et al., 2012). Although these techniques potentially enable quantification of NM distribution in an exposed organism, they do so only to the tissue or organ level. Direct imaging techniques on the other hand offer powerful methods for visualising NMs within tissues, at cellular and even sub-cellular levels. There are few well-defined techniques, however, for accurately imaging or characterising nanoparticles within a biological matrix. Electron microscopy (EM) has sufficient resolution to determine nanoparticle localisation within a tissue (Cheng et al., 2007; Mouchet et al., 2008; Soto et al., 2005), and high-resolution transmission electron microscopy (TEM) can provide detailed information on the structure of individual nanoparticles (Petri-Fink et al., 2008). EM techniques can also be combined with energy-dispersive X-ray spectroscopy (EDX) analysis to identify the nature of any metal constituents of the NMs. However, samples for both TEM and scanning electron microscopy (SEM) require preparation methods and imaging conditions which can create artefacts within the sample, such as NM aggregation, that do not have an exposure-related aetiology. These techniques also do not allow for imaging of live tissues. Furthermore, TEM can generally only be used for metallic particles that are electron dense as non-metal coatings or shells lacks adequate contrast (Fan et al., 2007). An exception to this is energy filtered transmission electron microscopy with electron energy loss spectrum imaging that has been used successfully to image single-walled carbon nanotubes (SWCNTs) in cells (Porter et al., 2007a,b).

Dark-field single optical microscopy has been applied successfully to track uptake of Ag NMs in real time into zebrafish embryos (Lee et al., 2007) and into nematodes (Roh et al., 2009) and this technique has nanometre resolution. However, the need for high intensity illumination can lead to photodamage, and the sample has to be extremely pure as contaminants can cause major interference. Furthermore, this technique has minimal tissue penetration.

Confocal microscopy, a linear optical technique has been applied successfully to visualise the bio-distribution multi-walled carbon nanotubes (MWCNTs) in zebrafish (*Danio rerio*) embryos (Cheng et al., 2009b) and polystyrene nanoparticles in hepatocytes (Johnston et al., 2010b). The disadvantage of standard confocal microscopy, however, is the requirement to stain the sample to provide contrast or, fluorescently label the nanoparticles (as in the studies of Cheng et al., 2009a; Johnston et al., 2010b), which may

change the nature of the particle (including their toxicity). Confocal techniques also lack spatial resolution (approximately 0.5  $\mu\text{m}$ ) and although they have sufficient depth penetration for studies on cultured cells, they are limited in depth penetration for most applications on whole tissues and *in vivo* imaging.

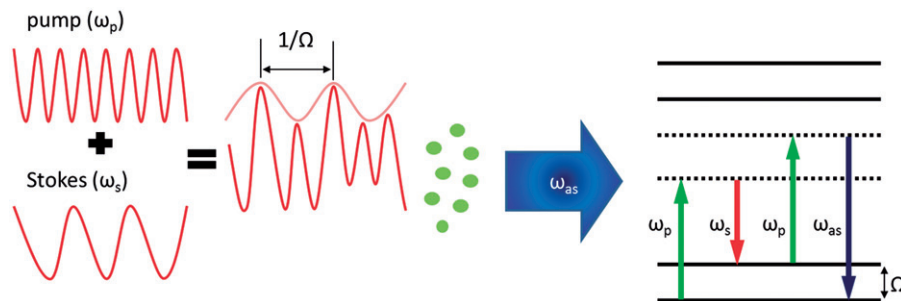
Some of the most recent techniques for visualising NMs utilise the specific intrinsic properties of the nanoparticles themselves to assist visualisation. Examples of these properties include the plasma oscillations resonating within the electromagnetic spectrum for gold nanoparticles (Murphy et al., 2008), and low activation energy from the valence to the conduction band and subsequent high quantum yield for quantum dots (Gonda et al., 2010; Jia et al., 2010). Of course, these methods are limited to specific types of nanoparticles with conductive properties.

In theory, CARS microscopy offers all of the desired features for imaging uptake and fate of engineered nanoparticles, including high selectivity (or contrast) and high sensitivity for NMs, the ability to image whole and sectioned cells, an ability to visualise cell structure, label-free detection, non-invasive, yield complimentary chemical information, high accuracy, reproducibility and high throughput. The strength of the CARS technique is its ability to detect, within a diverse range of complex biological matrices, a wide variety of nano-sized structures, such as those composed from ceria, titania and zinc oxides, silicon, gold, silver, carbon, diamond and polymer materials. Not all NM types have been investigated thoroughly using CARS and the list given is for materials for which there is published research and that provide positive image targets. Further research on other, including novel NMs, will likely yield a much wider compliment of materials suited for CARS detection methods. Although CARS can often differentiate between particle types, it cannot discern precise particle size (for further details and references see section on *Detecting NMs using CARS*). In this review, we first provide technical details to describe how CARS works, we then critically discuss applications for localising NMs in a variety of biological tissues, spanning isolated cells, excised tissue samples and whole live organisms, and finally we investigate future prospects for this technique as applied to the field of nanotoxicology.

### CARS microscopy

Microscopy techniques based on vibrational spectroscopy offer intrinsic chemical selectivity, as different molecules have specific vibrational frequencies. Infrared microscopy has seen widespread development for biological applications (Rodriguez et al., 2006), but is limited by poor sensitivity due to water absorption and low spatial resolution associated with the long infrared wavelengths.

Figure 1. The four wave mixing process of CARS utilises a pump beam, of frequency  $\omega_p$  and a Stokes beam,  $\omega_s$ . When the beat frequency ( $\omega_p - \omega_s$ ) is tuned to match that of a Raman active vibrational mode,  $\Omega$ , this generates a strong anti-Stokes signal at  $\omega_{as} = 2\omega_p - \omega_s$ .



With Raman scattering a great deal of chemical information can be obtained by examining light that is scattered by molecular vibrations. Raman scattered light is emitted at a slightly shifted wavelength with respect to the incident light; the shift in energy corresponding to the vibrational frequency of a molecular bond within the sample. The wavelength of the Raman scattered light can either be longer (Stokes shifted) or shorter (anti-Stokes) than the excitation wavelength. Recording the spectrum of Raman scattered light excited by a single incident wavelength produces a series of signal peaks each corresponding to a vibrational frequency unique to specific chemical bonds within sample molecules. Raman spectra provide a chemical finger-print of a sample that can yield a wealth of information about the chemical composition of a sample with regards to the chemical bonds present. Raman microspectroscopy has been extensively explored to map the chemical composition of biological samples and has found a broad range of biomedical applications (Evans & Xie, 2008) including, tumour diagnostics, DNA detection, bone mineral density and microendoscopy. The technique, however, suffers from the fact that Raman scattering is extremely weak (typical photon conversions for Raman scattering are lower than 1 in  $10^{18}$ ). Therefore, image acquisition times are long and often high laser power is required. These factors have limited the application of Raman microscopy in the study of living systems due to the combined factors causing photo-damage.

Far stronger molecular vibrational signals derived from chemical bonds can be obtained using coherent anti-Stokes Raman scattering (CARS), first demonstrated by Maker & Terhune (1965) for analysing the molecular vibrational spectra of combustion gases. In 1999, developments in ultrafast infrared lasers revived CARS microscopy as a tool for biological imaging (Zumbusch et al., 1999) and its application in bio-imaging has increased dramatically in the last ten years. However, CARS is affected by an electronic, non-chemically specific background such as those produced from solvents. This places limitation on the sensitivity and chemical specificity of the technique as the background signal can reduce the contrast from objects present at a low concentration. Therefore, CARS is most successfully applied to imaging cellular components where the chemical bond species of interest exhibit at a high concentration such as phospholipids, which contain a high CH bond density.

CARS microscopy derives its contrast from intrinsic molecular vibrations in a sample. The CARS process involves two lasers where the frequency of the first laser is constant, while the frequency of the second one can be tuned in a way that the frequency difference between the two lasers equals the frequency of the Raman-active or vibrational mode of interest. A pump beam at frequency  $\omega_p$  and a Stokes beam at frequency  $\omega_s$  interact with a sample via a wave-mixing process so that when the beat frequency  $\omega_p - \omega_s$  matches the frequency of a Raman active molecular vibration, the resonant oscillators are coherently driven by the excitation fields, thereby generating a strong anti-Stokes signal at  $\omega_{as} = 2\omega_p - \omega_s$  (Figure 1). Therefore, the molecules in

resonance produce a larger signal than those off resonance, providing a vibrational contrast in a CARS image. The non-linear CARS process uses pulsed laser sources and is generated via four-wave mixing (FWM) processes in which the signal intensity has quadratic and linear dependence on pump and Stokes powers, respectively.

However, the FWM signal of the CARS process is not the only contribution to the signal generation. Without vibrational resonances CARS can still occur through electronic motions which produce a non-resonant background signal. This non-resonant contribution is spectrally indistinguishable from the CARS signal. The non-resonant components are related to the sample's third-order electronic susceptibility and are independent of the frequency difference  $\omega_p - \omega_s$ , therefore do not provide any vibrational contrast and thus no chemical specificity. They are, in essence, a map of the electronic polarisability and density of a sample. For most biological imaging applications investigators strive to minimise the non-resonant contributions, however, the process that generates these non-resonant contributions can be exploited to derive image contrast from sub-wavelength NM which have enhanced non-linear electronic susceptibility, discussed later in more detail.

The problems associated with the non-resonant contribution in a sample, namely the generation of a background to the image, has driven the development of a number of methods to reduce this effect. One of the most effective involves detecting the CARS signal in the backwards direction, or epi-detected CARS (E-CARS, Volkmer et al., 2001). This means that a small scatterer or imaging target (with an axial length less than the anti-Stokes wavelength, approximately 300 nm) has a backwards signal that is comparable to the forwards signal (F-CARS, Cheng et al., 2001). Therefore small scatterers have a significantly higher contrast in the epi-direction than in the forwards direction. Conversely, only the larger cellular structures appear in the F-CARS images. When comparing the (identical) frames, the smaller scatterers present in the epi-generated image relate to black-holes or they are not present at corresponding locations in the forward-images, highlighting their complementary properties. An additional advantage of detecting two signals (F- and E-CARS) is the elimination of background noise present in the forward image that arises from the non-resonant electronic contribution to the CARS signal discussed earlier (Scown et al., 2010).

The CARS technique requires specialist equipment and user expertise, however, the practicalities of imaging samples using CARS microscopy are relatively straightforward. Figure 2 shows a schematic set-up of the equipment for CARS. Most of the limitations placed upon imaging biological material with CARS relate to fixing, storage and transport of the sample. CARS microscopy is extremely sensitive to degradation of a sample, and chemical modifications are detected before any physical changes become apparent. Because of this for excised tissues, in some instances, fixatives are required. Use of fresh/live biological samples avoids (or much reduces) issues that might relate to

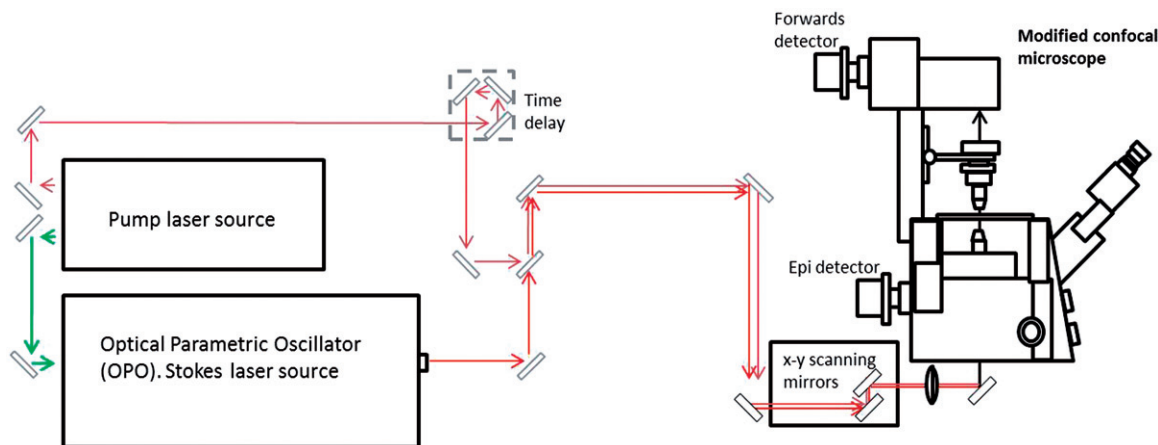


Figure 2. Schematic diagram of the CARS equipment, showing the two laser sources (pump and Stokes) and the location of the detectors at the end of the beam path.

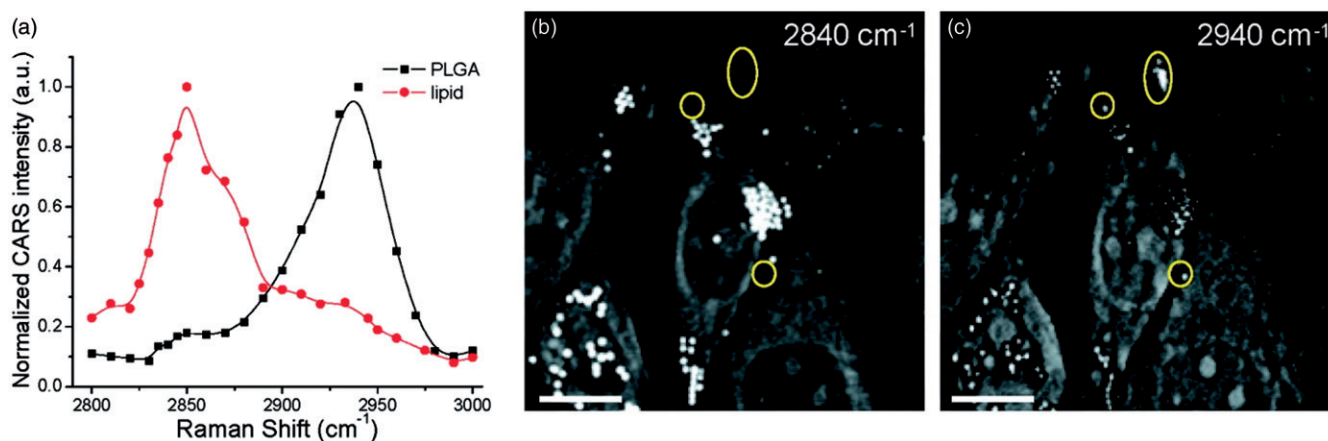


Figure 3. Chemically selective imaging of intracellular lipid bodies and extracellular PLGA particles by CARS microscopy. (a) CARS spectra of a PLGA film and lipid bodies in KB cells. The two peaks at  $2940\text{ cm}^{-1}$  and  $2840\text{ cm}^{-1}$  arise from  $\text{CH}_3$  stretch vibration in PLGA and  $\text{CH}_2$  symmetric stretch vibration in lipid bodies, respectively. (b) CARS image at  $2840\text{ cm}^{-1}$ . (c) CARS image at  $2940\text{ cm}^{-1}$ . The CARS signals were detected in the forward direction. The lipid bodies produced a stronger signal at  $2840\text{ cm}^{-1}$ , whereas the PLGA particles (in yellow circles) could only be seen at  $2940\text{ cm}^{-1}$ . These data show that PLGA NPs did not enter KB cells after 3 h of incubation with NPs. Scale bars represent  $10\text{ }\mu\text{m}$ . Reprinted with permission from Xu et al. Copyright 2008 American Chemical Society.

deterioration of the sample. Challenges when applying CARS with live specimens revolve around specimen immobilisation, arising either from mild convection currents that are generated from localised thermal events in culture media or water, created by the laser source or from an actively moving specimen. Various protocols and customised slides have been designed for different samples in attempt to circumvent these problems. For small animals that are highly mobile and for which adherence options onto a surface are not appropriate (as works for cell cultures) or for which physical confinement does not work, use of a mild and reversible anaesthetic in an immobilisation option.

### Detecting NMs using CARS

Features of the CARS process can amplify various components of NMs that facilitate specific imaging of the material. Although some non-resonant contributions reduce image contrast some, however, are useful. Materials with naturally large non-resonant susceptibilities provide excellent contrast using CARS spectroscopy. This is due to their strong electronic resonances which generate extremely strong F- and E-CARS signals. This occurs for metal oxide NMs, as demonstrated by Moger et al. (2008). In addition to exhibiting markedly different chemical properties

from their bulk materials, NMs can also exhibit enhanced optical properties that are often accompanied by an enhancement of the non-linear optical properties (Wang et al., 2011). Moger et al. (2008) showed that this enhancement can be exploited in metal oxide NMs to produce large FWM signals, thus allowing excellent visualisation of these materials. The heightened non-linear response of some NMs allows for the location of particles far smaller than the linear scaling of the signal from bulk material would suggest.

For non-metallic NMs, detection using CARS works by tuning the Stokes beam wavelength to match the frequency of a specific Raman active vibration unique to the material under investigation. Very recently single nanodiamonds were imaged using CARS microscopy tuning into their specific diamond ( $\text{sp}^3$ ) vibrational resonance (Pope et al., 2014). Some polymer NMs can also be detected in this way; for example, poly(lactic-co-glycolic acid) (PLGA) particles, can be chemically distinguished by tuning into their  $\text{CH}_3$  bonds away from the more ubiquitous  $\text{CH}_2$  vibrational mode (Xu et al., 2008, Figure 3). Similarly, polystyrene nanoparticles can also be distinguished relatively easily by exciting their aromatic C-H stretching vibration to provide specific detection away from the typical lipid signal present in most biological samples (Cole et al., 2013; Tong et al., 2007).

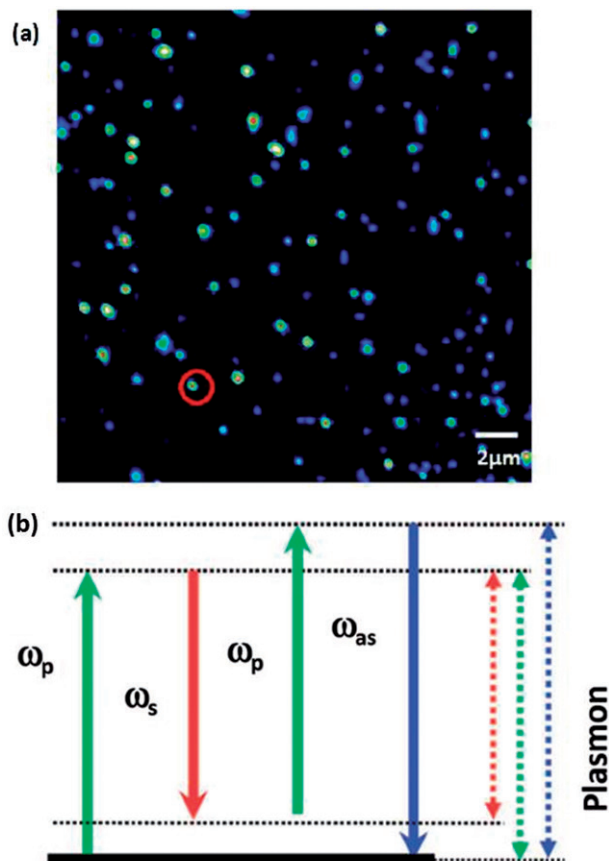


Figure 4. (a) Imaging gold nanorods (98 nm with an aspect ratio of 3.6) with FWM signal. (b) Energy schematic of FWM from gold nanoparticles. When the plasmon resonance wavelength matches the pump, Stokes or anti-Stokes wavelength, FWM is expected to be enhanced. Reprinted with permission from Jung et al. Copyright 2009 American Chemical Society.

However, some polymeric NMs that are typically fabricated to be biocompatible are difficult to detect using CARS, due to their lack of unique bonds from those in natural lipid sources that can be resonantly targeted and exploited. Biological molecules such as DNA have also been visualised with CARS at the nanoscale through assigning the resonant frequency to the ring-breathing mode of a diazole adenine molecule in the DNA (Ichimura et al., 2004).

The quantum size effects of some NMs can also contribute to an enhanced CARS response. Silicon, for example, has non-linear susceptibilities that are among the highest known for solid state materials (Wynne, 1969) thus nano-sized silicon has been highlighted as a potential tool in imaging applications (Park et al., 2009). Similarly, strong responses have also been established for quantum dots (QDs, Jain & Lind, 1983). Although some materials, such as gold, do not have any Raman active bands and the FWM signal cannot be enhanced by vibrational resonance, their optical properties are dictated by the presence of surface plasmons and coherent electron oscillations that occur at the material interfaces can facilitate their detection via CARS. As exemplified by gold nanorods (98 nm in length, with an aspect ratio of 3.6), FWM occurs strongly when the pump laser wavelength is tuned to be resonant with the longitudinal plasmon resonance wavelength (Jung et al., 2009, Figure 4) and the coherent FWM signal arises from a plasmon-induced enhancement of gold's non-linear susceptibility. This leads to an intense signal that can be readily isolated from any resonant CARS signals in the surrounding medium. This is a property which

makes gold very attractive as contrast agents in live biological samples (Garrett et al., 2011).

CARS has also been applied to the imaging of carbon nanotubes. These materials provide strong FWM (Lefrant et al., 2008), which can be enhanced making a sensitive probe for the non-linear electronic response of nanoscale objects such as nanotubes. Strong signals are, therefore, expected from SWCNTs which generate FWM when the excitation beams are resonant with electronic transitions of the nanotube (Kim et al., 2009). In contrast with SWCNTs, the optical nonlinearity of graphene means that it does not show resonant behaviour as a function of excitation wavelength. It does, however, exhibit a very strong optical nonlinearity from the interband electron transitions in the near-infrared spectral region enabling its detection using CARS (Hendry et al., 2010).

A major challenge to the application of CARS microscopy in nanotoxicology is the fact that its spatial resolution is  $\approx 200$  nm and many NMs of interest in nanotoxicology are less than 10 nm in diameter, albeit that many NMs in biological tissue will be present as aggregates. Despite this apparent limitation for using CARS in nanotoxicology, particles smaller than 200 nm are still imaged successfully due to the enhanced non-linear response from NMs, compared to the same larger-sized material. Indeed particles of 5 nm Ag provide sufficient signal to be detected using CARS. The limitation arises when trying to determine the size of the smallest detectable NM or NM aggregate, which is not possible, due to the point-spread-function of the imaging system exceeding the size of an individual nanoparticle (Rodriguez et al., 2006). This leads to variation in intensity of the signal which manifests as a varying brightness in the image from particles appearing to be of similar size, but that are below the resolution limit. This complication could be alleviated if it were possible to image a single nanoparticle with CARS and subsequently record its brightness.

In summary, CARS can be applied to visualise a wide range of particle types including, polymer, carbon and metallic NMs, exploiting their innate properties. Some of the unique attributes of NMs can be enhanced by the CARS process and consequently provide excellent contrast and targets for visualisation and in turn for the localisation of these materials within a biological matrix.

### Imaging biological material with CARS

A fundamental requirement for the imaging of NMs within tissues is the ability to identify the structures of the biological materials themselves, the tissues, cells and cellular components. This information is clearly required to localise the NMs within the tissue matrix before any measurements, comparisons, aberrations or diagnostic data can be drawn. Utilising the variation in intrinsic biochemical properties of a tissue/cell, CARS enables visualisation of a range of structural features. As the contrast is provided by the chemical composition of the biological sample (i.e. what bonds are targeted), CARS images provide more information than a corresponding transmitted light image. This range of chemical selectivity is demonstrated with the excitation and identification of phosphate groups, C–O bonds of DNA, C=C and C–H bonds, and amide bonds (Cheng et al., 2002a,b; Hashimoto et al., 2000; Volkmer et al., 2001). This enables imaging within a cell of the cytoplasm or nucleus (Figures 3b, c and 5a), without the need for any non-native contrast agent or pre-processing of the sample which could interfere with endogenous biological processes of interest. An important point to note, however, is that when using CARS to image a particular molecular species, these functional groups will appear in a variety of different biomolecules, and the image will thus require further information or interpretation to clarify precise localisation.

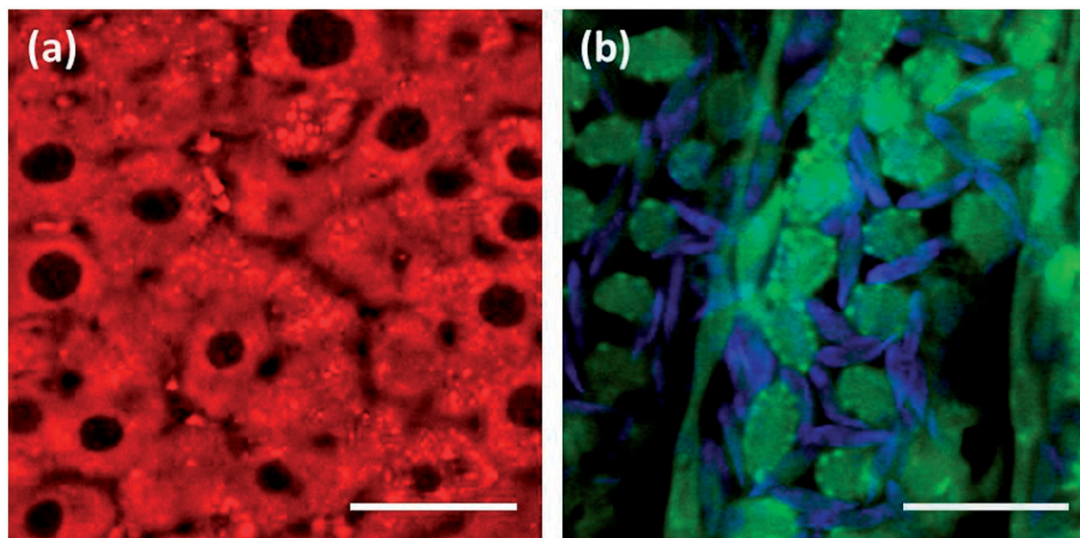


Figure 5. (a) Mouse liver tissue imaged with epi-CARS with contrast derived from the  $\text{CH}_2$  resonances at  $2845\text{ cm}^{-1}$ . Here the image is taken in the  $z$ -plane that runs through the centre of the cell as the nucleus is in focus. Reproduced from Lalatsa et al. (2012). (b) A close up of a gill arch excised from a rainbow trout reveals the resolving ability of the CARS technique to delineate structural differences within a tissue sample. The blood cells circulating in the tissue are visualised in a blue false colour. Scale bar represents (a) 40 and (b) 50  $\mu\text{m}$ . Reproduced from Moger et al. (2008).

CARS is able to image with sufficient resolution at the cellular level for discerning alterations in cellular features and morphological aberrations in an exposed sample, particularly as applied to cells in culture. The spatial resolution of CARS of 200 nm, however, clearly prevents imaging of the majority of organelles within a cell, reducing the detail of the image.

Imaging at the cellular scale with CARS is not limited to cells in culture and has been applied effectively also to characterise structural and cellular features of an isolated tissue sample. An example of this is portrayed in Figure 5(a and b) fish gill arch from a rainbow trout showing blood cells circulating within the capillaries of the tissue. This exemplifies CARS's effective application to excised tissues and the potential for accurate localisation of NM within organs after an exposure. Recently, CARS has been applied to excised gill and foregut tissue in shore crabs (*Carcinus maenas*) exposed via the diet and via the water to assess the uptake of microplastic pollution (Watts et al., 2014).

Imaging methods that require manipulation of the immediate environmental conditions can impact adversely on biological tissue and photo damage is of particular significance for a number of microscopy techniques. The use of infrared excitation and the fact that the CARS process produces large and directional signals, however, not only gives CARS an increased depth penetration over conventional optical microscopy (Helmchen & Denk, 2005), but importantly, reduces both the average excitation power needed and in turn the amount of photodamage to cells and tissues. The wavelengths used in CARS are also less phototoxic because of the lack of significant endogenous absorbers in most tissues (Svoboda & Block, 1994). This minimises the risk of photobleaching with CARS that is common in fluorescence based microscopy, and can affect the viability of live cells and tissues. Thus CARS imaging has significant advantages over other many other microscopy techniques for imaging tissues with minimum biological effect.

Understanding of the CARS output is of vital importance for image interpretation. Subsequent contrast superimposition to understand the image, such as the biodistribution or penetrance of NMs, requires intelligent processing by the user that is

sensitive to the original image. As both chemical and structural detail are generated, visual information from biological structure must be correlated to tissue or cell type and be relevant to the tuned excitation wavelength.

### CARS imaging of NMs in biological matrices

Precise localisation of NMs within a biological matrix is extremely useful but demanding for the imaging technique. The first challenge is having sufficient spatial resolution to locate particles within a cell and is ideally combined with a 3-dimensional sectioning capability. The CARS signal is sufficiently precise to be able to allow this. Originating from a very small volume within the sample, at the focal point where the excitation density is highest (Cheng et al., 2002b), this precise signal facilitates the spatial partitioning of biological structures with molecular details in 3D. The second major challenge is that the imaging modality can detect and derive sufficient contrast from both the biological matrix and the NMs, which are highly varied targets. Important in this respect is the accuracy of CARS imaging compared to tracing NM localisation using fluorescent tags or markers. This is because CARS directly images the particle itself and not the label attached to aid its tracking, as some other microscopy methods require, ensuring determination of the precise localisation of a NM. Potentially where tracers/fluorescent markers are used, the label can become dissociated from the particle giving a false positive. As an example of this, in a study by Xu et al. (2008) a lipophilic dye was shown to be released from nanoparticles into the surrounding extracellular medium before the dye was taken up by cells. In this instance confocal microscopy and data from a fluorescence activated cell sorter (FACS) produced data that suggested nanoparticle uptake, yet CARS assessment showed the absence of particles within the cells, giving a different conclusion; indicating a lack of nanoparticle uptake.

The FWM process of CARS is a key when imaging NMs within a biological matrix, where the non-resonant susceptibilities of NMs can be used to distinguish them from the stimulated vibrational contrast from commonly targeted molecules such as lipids. Thus, the ability to tune the excitation wavelength away from the natural

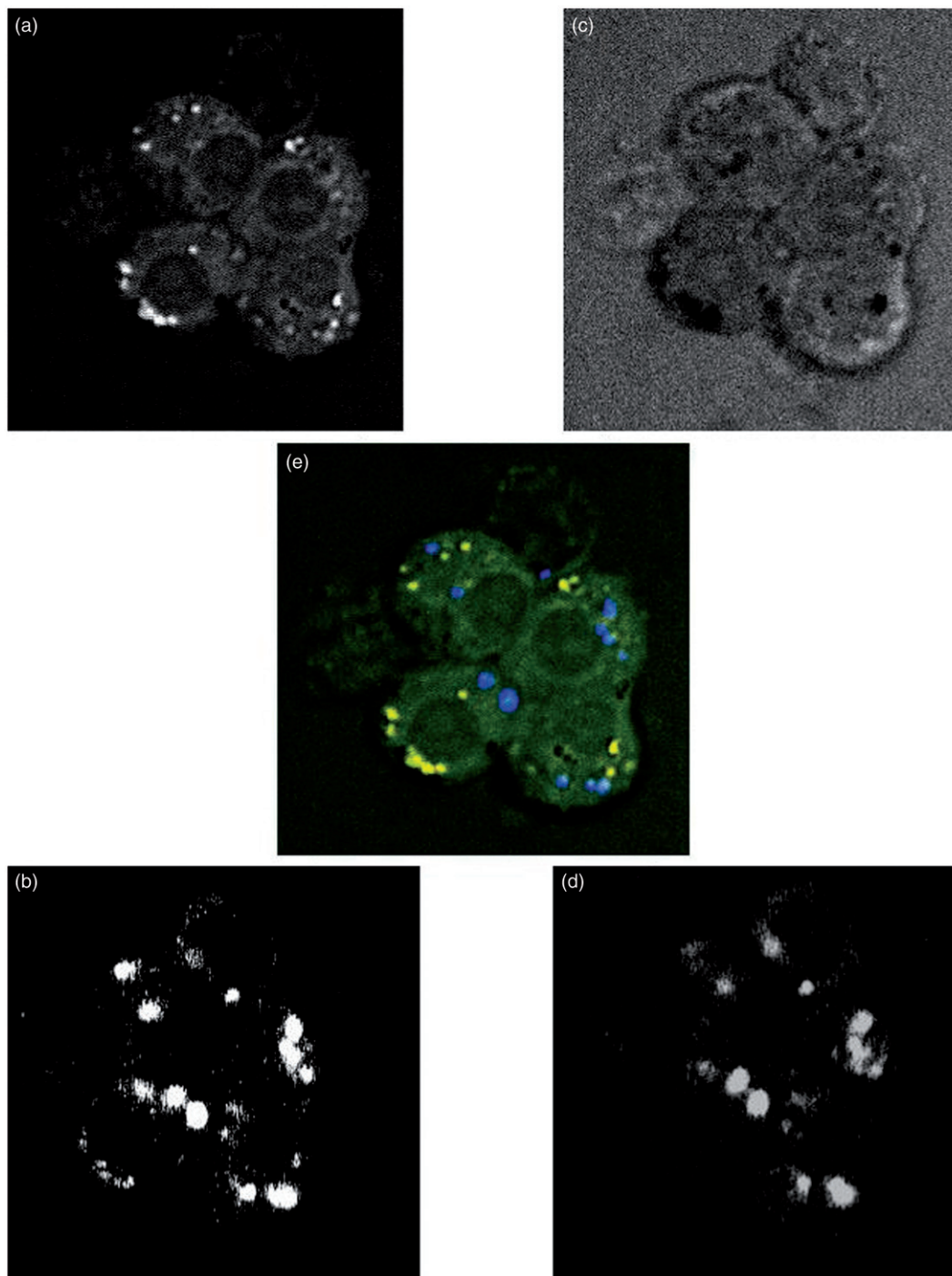


Figure 6. Rainbow trout hepatocytes after exposure to 10 nm  $\text{CeO}_2$  NMs. Imaging at the C–H exciting wavelength of  $2840\text{ cm}^{-1}$  (a and b) lipid dense structures are detected in both forwards (a) and backwards (b) directions as bright white spots. The same images at a wavelength of  $2955\text{ cm}^{-1}$  (c and d) negatively contrast C–H bonds which appear black spots in the forwards direction (c) or not at all in the backwards direction (d). Thus, the bright spots that are still generating a strong signal at both wavelengths are NM. These data can be combined to present an image where the lipid fluorescence and the signal from the NMs are distinguished (e), here the yellow colouration represents the signal obtained from excited C–H bonds in lipid dense structures, the green depicts the cellular structure and the blue is generated from strong E-CARS signal of the broad spectrum. Additionally uptake of NMs is ascertained by the CARS signal being present in the same imaging plane as cellular structures such as the nucleus. Scale bar represents  $20\text{ }\mu\text{m}$ .

vibrational resonance of a sample (used for structural information), allows for confirmation of the presence of NMs which produce a strong signal across a broad wavelength spectrum. This is because the C–H bonds will not produce non-resonant contributions in the image (Akimov et al., 2009) and off resonance, in the biologically silent region of the Raman spectrum, the only signal generation will come from the NMs.

This ability to distinguish NM from biological material has been demonstrated in the studies on the uptake of various NMs

into primary cultured trout hepatocytes by Scown et al. (2010), where tuning the excitation wavelength off resonance for C–H bonds was used to confirm the remaining signals were derived from NMs. To illustrate this further, Figure 6 shows imaging at two different Raman vibrational frequencies to detect nano-sized cerium dioxide ( $\text{CeO}_2$ , nominally 10 nm) particles in primary isolated rainbow trout hepatocytes. Imaging at the C–H exciting wavelength of  $2840\text{ cm}^{-1}$  (Figure 6a and b) identifies lipid dense structures in both forwards and backwards directions (seen as



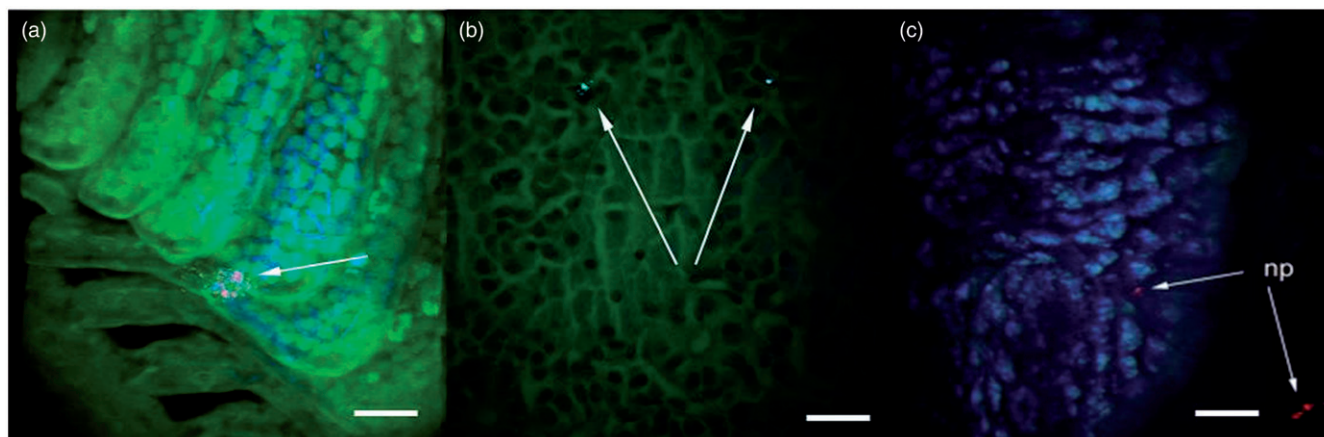


Figure 7. CARS images of (a) the gill arch of a rainbow trout, reproduced from Moger et al. (2008), (b) rainbow trout kidney tissue (Scown et al., unpublished) and (c) gut of *Arenicola marina*, reproduced from Galloway et al. (2010). All images taken at  $2850\text{ cm}^{-1}$  ( $\text{CH}_2$  stretching) showing the presence of titanium dioxide nanoparticles [indicated by arrows; (a) 25–70 nm, (b) and (c) crystallite size 23.2 nm] associated with the tissue. Scale bar represents  $100\text{ }\mu\text{m}$ .

white spots in the images presented). When imaging at a wavelength of  $2955\text{ cm}^{-1}$  (Figure 6c and d) this negatively contrasts C–H bonds, which appear as black spots in the forwards direction and are not present in the backwards direction. This facilitates the ability to distinguish between endogenous scatterers such as lipids and NMs where the strong excitation signal detected in the system is generated across both wavelengths. These images can be merged in “false colour” to highlight the different signals and identify the presence of NM in the tissue (Figure 6e).

This tuning method of CARS removes the possibility of confusion between native and non-native scatterers, such as lipids and NMs, respectively, within the sample. This technique can be applied for any NM within the system, although, particles that require exploitation of their specific properties, will only be visible at their particular stimulated wavelength. An example of this is for gold nano-shells (Garrett et al., 2011).

CARS has now been applied in a number of ecotoxicology studies to trace the uptake of various NMs into biological tissues with the potential to assess for the effects of material properties, capping agents and environmental conditions on the mode of uptake and biodistribution; information which is currently lacking or difficult to attain from the current literature (Tantra & Knight, 2011). Examples of this include Moger et al. (2008) and Johnston et al. (2010a) utilising CARS to localise  $\text{TiO}_2$  NMs in the gills of rainbow trout (*Oncorhynchus mykiss*) after a water borne exposure. These studies established uptake and penetrance of the NM on a cellular scale in a fragile sample (Figure 7a). CARS has also been applied successfully to *Arenicola marina* (Galloway et al., 2010, Figure 7b) and excised rainbow trout kidney tissue (Figure 7c) to confirm  $\text{TiO}_2$  nanoparticle presence, for particles ranging between 23 and 70 nm in size.

Medical research using CARS includes into nano-drug delivery systems (e.g. Belsey et al., 2014). Visualising the distribution of the particle within surrounding cellular structures allows for a greater understanding of nano-drug delivery potential, with great potential benefits for measuring the distribution, retention and depuration of novel drug delivery systems. The critical aspect of the CARS system that allows imaging deep into scattering tissue, as exemplified above, are the excitation wavelengths being near infra-red, which result in low scattering and thus an increased penetration, up to several hundred microns, into the sample. Importantly, from these examples, is the achievement of rapid, non-invasive NM detection that can complement and reinforce concurrently run data sets on other toxicological end-points of interest.

It should be made clear that the CARS process is principally qualitative and a notable drawback is that the CARS signal does not scale linearly with compound concentration making quantitative analysis problematic, although not impossible. Quantitative capabilities of CARS are most limited with less abundant scattering targets.

Ultimate identification of particle location within a biological matrix relies on the 3D sectioning capability of CARS. For hepatocyte exposures (Scown et al., 2010), internalisation of copper NMs was confirmed by taking a series of 2-dimensional images through the  $x$ - $y$  plane, each separated by  $0.25\text{ }\mu\text{m}$  in the  $z$ -direction. By creating this “ $z$ -stack” and 3D reconstructed image, the origin of the NM signal was found to be centred within the boundaries of the cell, confirming penetrance of the material into the cell (Figure 8a). This method to ascertain internalisation is not restricted to single cells. Moger et al. (2008) used this technique with gill tissue and Fabrega and colleagues (unpublished) made preliminary assessments on the retention of zinc oxide ( $\text{ZnO}$ ) bulk sized particles within the gut of a *Corophium volutator* determined by a 3D reconstruction of the gut and hepatopancreas (Figure 8b) before further study (Fabrega et al., 2011).

### CARS applied to the detection of NMs in whole organisms

Live samples exhibit all the biological processes that interact with or are stimulated by the presence of NMs. This makes real-time imaging a perfect snap-shot of the true functionality and behaviour of the NMs *in situ*. In addition to imaging of cells in culture and excised tissue, CARS has now also been successfully applied to imaging of NMs in live intact organisms. The technique has been applied to organisms spanning bacteria to invertebrates to fish. In work on bacteria CARS has been used to identify anthrax spores in a sealed envelope, tuning in to dipicolinic acid which is a major chemical component of bacterial endospores (Arora et al., 2012). Host-pathogen interactions have also been investigated using CARS, including the relationships between hepatitis C virus RNA and alterations in host-cell lipid metabolism (Nan et al., 2006) as well as understanding the virulence factors associated with host interaction such as the upregulation of proviral genes (Blais et al., 2010).

A review on NM hazard assessment concluded, the fate and behaviour of NMs that modulate their environmental impact is the

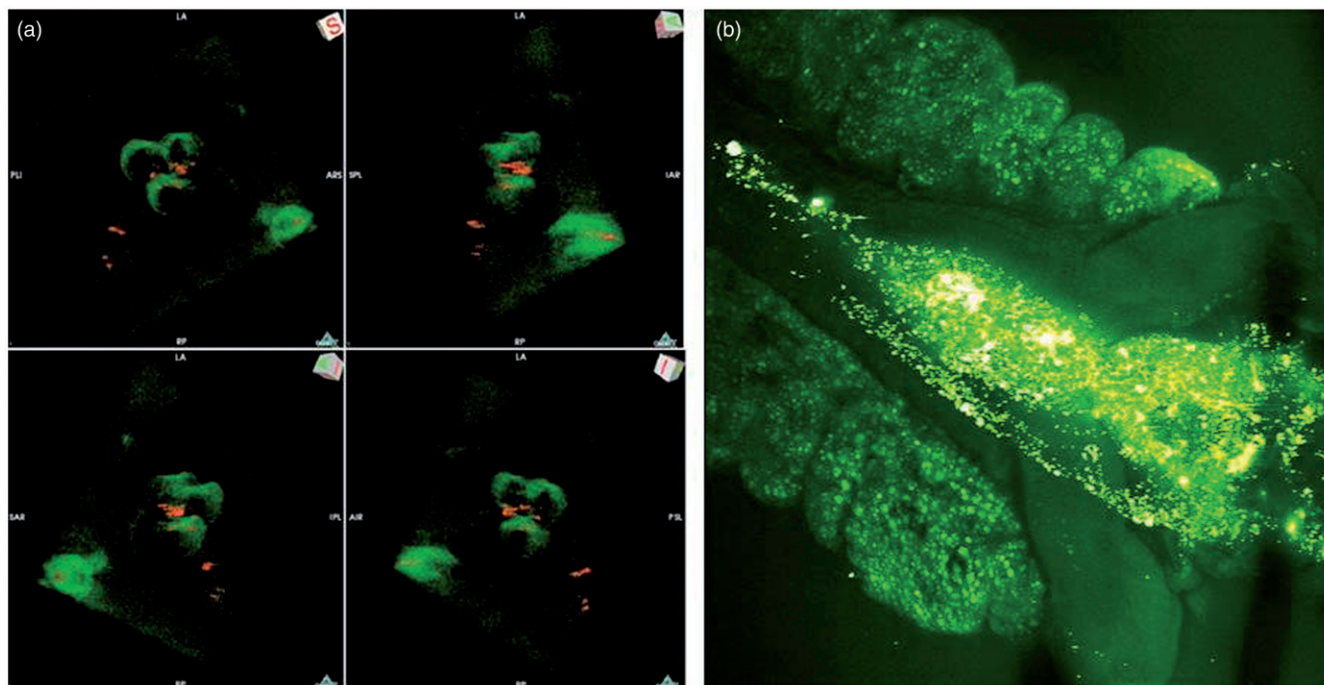


Figure 8. Z-stacks of both cells and whole organisms can be reconstructed to provide 3-dimensional analysis of a sample which is a useful approach to help establish nanoparticle localisation and biodistribution within biological tissue. Here; (a) Cu nanoparticles, indicated in red, are contained within the cultured hepatocyte cells and (b) ZnO micron-sized particles are shown to be within the gut of a *Corophium volutator* from a 2D slice of a 3D reconstruction. Animated versions of the 3D images are presented in the supplemental material.

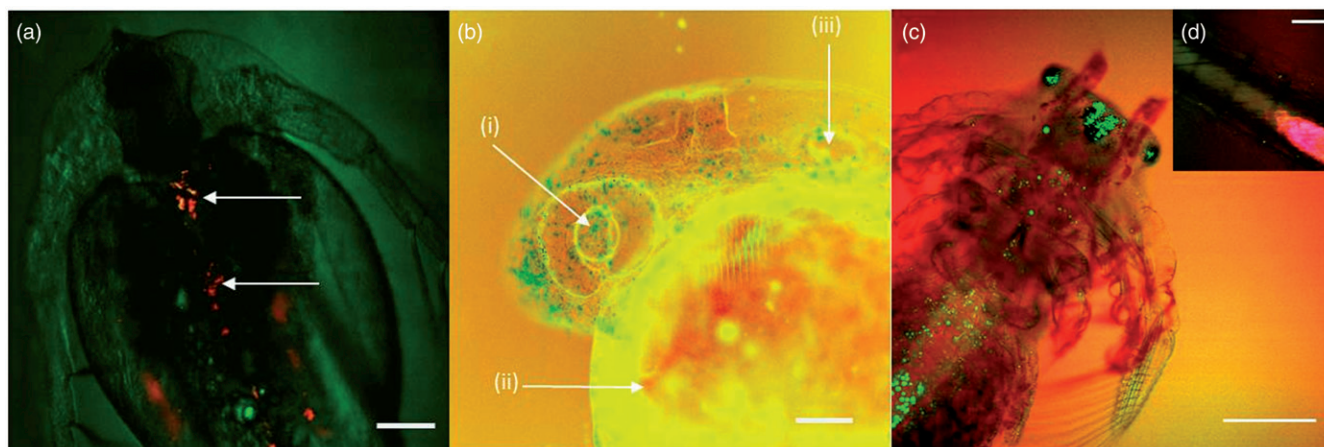


Figure 9. CARS images demonstrating the ability to localise nanomaterials in exposed live organisms, and signals that are spectrally unassigned and can complicate NM detection. (a) ZnO particles (crystallite diameter 41.5 nm) here depicted in red (arrowed), retained in the gut of a daphnia. (b) A zebrafish embryo microinjected with 7 nm Ag NMs at the one cell stage. Green components of the image are the Ag NMs dispersed throughout the organism. The eye (i), yolk sac (ii) and ear (iii) are marked for orientation. (c and d) Signals derived from algae food source in fairy shrimp (c) photosynthetic algae in the gut of a fed animal showing a strong non-resonant contribution (depicted in green) and (d) the overwhelming signal (here in pink) from ingested algae in the hind gut. Scale bars represent 100  $\mu\text{m}$  (a and b) and 50  $\mu\text{m}$  (c and d).

“one black box (that) remains to be opened and understood” (Kahru & Dubourguier, 2010). Subsequent to realistic exposure routes, visualisation of NMs with CARS in live organisms can elucidate cellular partitioning and excretion routes. Invertebrates are ideal organisms to assess this and CARS has predominantly been applied to work with model species such as *Caenorhabditis elegans* (e.g. Hellerer et al., 2007) and with *Daphnia* and *Corophium* for studies on NM biodistribution (Larner et al., 2012). Figure 9(a) illustrates ZnO nanoparticles (crystallite diameter 41.5 nm) uptaken and retained in the gut of a daphnid. This image permitted viable assessment of further propagation of

these NMs from the gut into other tissues (Fabrega et al. unpublished data). In a study by Larner et al. (2012) CARS analyses showed Zn accumulated within both the alimentary tract and the hepatopancreas from all  $^{68}\text{Zn}$  exposures, but not in control organisms.

Some invertebrates provide a separate challenge by the way of non-resonant signal contributions from their diet. Algae, which contain the pigment chlorophyll, fluoresce and are a natural optical absorber of light and as such disrupt the imaging of invertebrates when algae are present within the gut. Figure 9(c) and (d) demonstrate the overwhelming non-resonant signal of

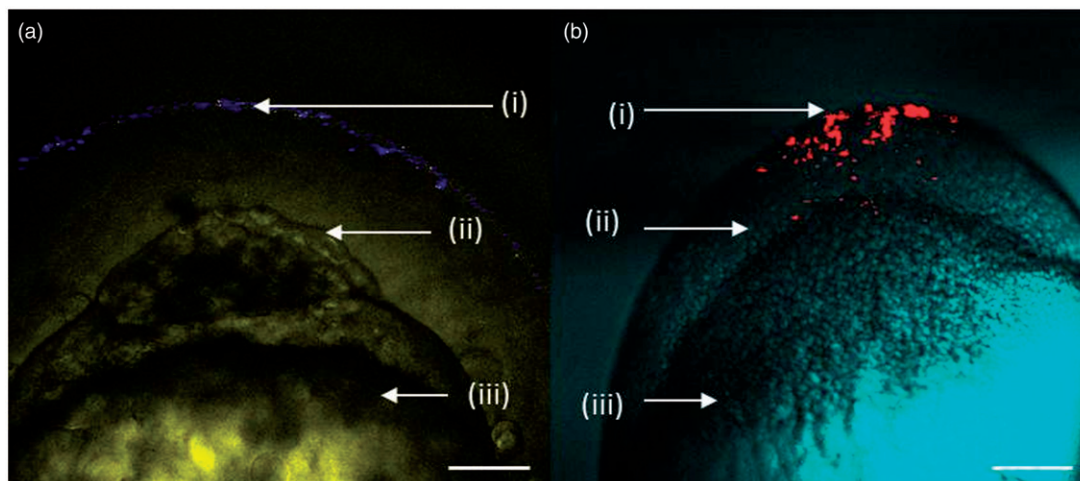


Figure 10. Zebrafish embryos microinjected at the one cell stage with (a) 5 nm  $\text{CeO}_2$  nanoparticles (i, contrasted blue), imaged at 3.5 hpf and, (b) 7 nm Ag nanoparticles (i, red) imaged 6 hpf. Both images are visualised at  $2850\text{ cm}^{-1}$  – the  $\text{CH}_2$  excitation frequency. (ii) Indicates a mass of dividing cells and (iii) the yolk sac. Scale bars represent  $100\ \mu\text{m}$ .

ingested photosynthetic matter in the gut of fairy shrimp (*Thamnocephalus platyurus*). Here the signal generated from algae residing in the digestive tract did not allow distinguishing of any NM present. This difficulty can be overcome to allow imaging of plant material containing photosynthetic pigments (Mansfield et al., 2013) but is technically challenging. CARS has recently been successfully applied to a fixed algal sample to visualise uptake of 106 nm Ag NM (Ribeiro et al., 2014).

In fish, species such as zebrafish are of particular interest due to their wide use as a model species in nanotoxicology and developmental research. The ability to image NMs in a live zebrafish embryo or early stage larvae would add significantly to studies on fate, transport and effects of NM in fish. Studies, injecting various NMs into one cell stage zebrafish embryos have shown that CARS can be applied to detect various metal based NMs within fish embryos. Figures 9(b) and 10 illustrate the distribution of Ag nanoparticles (7 nm) and  $\text{CeO}_2$  NMs (5 nm) in a zebrafish embryo at 24 hours post fertilisation (hpf) after injection of the NM at the one celled stage. For these injections, the cerium was seen to associate with the chorion (Figure 10a) and was not retained in the embryo, contrasting with that for Ag particles (Figure 10b), which were retained within the embryo and was distributed throughout the dividing cells, CARS has also been successfully employed to image embryos after aqueous exposures to NMs (Osborne et al., 2013), where there was no evidence for Ag particles crossing the chorionic membrane in exposed embryos. In combination with other data the CARS images suggested that Ag ions played a major role in the toxicity of Ag NMs.

Direct imaging data derived from CARS can facilitate more intelligent interpretations on tissue fate and how this relates to any biological effects seen and can also be used to gain greater understanding of real-time NM kinetics. Whole organism imaging with CARS allows for comprehensive assessment of nanoparticle fate and behaviour for that exposed organism. Whole organism imaging with CARS, however, is limited to animals of a relative small size and also depends on the opacity of its surface. Some organisms such as zebrafish pigment cells, including melanophores and iridophores that develop from 25 hpf generate signals under CARS that are indistinguishable from the broad signal wavelength from many metal NMs.

Collectively, the studies highlighted here show CARS has been applied successfully to a number of different *in vivo* systems for tracing material uptake and distribution within cellular and tissue

matrices, including for real-time analyses. CARS is arguably best applied in conjunction, however, with other techniques such as radio labelled NMs (Larner et al., 2012) to provide both qualitative and quantitative analysis of NM exposure and in turn produces a more holistic understanding for those exposures.

### Future applications

Since the re-emergence of CARS over 10 years ago, non-linear label-free imaging based upon Raman scattering has been developed further with stimulated Raman scattering (SRS). This technique eliminates non-resonant background because, when the Raman shift does not match any vibrational resonance, there is no generated signal (Freudiger et al., 2008). This is in contrast to CARS, which exhibits a strong spectral background independent of the Raman shift. However, it is precisely this non-resonant spectral background of CARS that provides the contrast for imaging metal NMs. An ideal set-up for imaging NMs in exposed cells and tissues is forwards detection of SRS with backwards detection of E-CARS. Further applications of CARS include in the area of nanotherapy and drug delivery that utilise the nano-sized properties of the NMs to improve efficacy, safety and targeting (reviewed in Caldorera-Moore et al., 2010). CARS provides a system allowing for assessing the performance of drug delivery particles in terms of uptake and distribution throughout a tissue. CARS has the potential also to assess for markers of toxicity, with the ability to detect chemical changes as a result of NM exposure. These might include some common toxicological endpoints measured subsequent to an NM challenge, such as changes in protein concentrations in oxidative stress reactions or as by-product of free radical generation. Thus, the CARS has future prospects not only for the detection of NM taken up into exposed organisms but also, in parallel, assessing for potential harm caused by these materials.

### Acknowledgements

The authors thank J. Shears and G. Paull and for technical support and N. Garrett and J. Mansfield for imaging expertise.

### Declaration of interest

The authors declare no conflict of interest.

This work was supported by the Natural Environmental Research Council (NE/H013172/1) and EU FP7 Large Collaborative Project NanoMILE (Grant Agreement No.310451) to CRT, and from the EPSRC (grant numbers EP/G028362/1 and EP/G061564/1) to JM.

## References

- Akimov D, Chatzipapadopoulos S, Meyer T, Tarcea N, Dietzek B, Schmitt M, et al. 2009. Different contrast information obtained from CARS and nonresonant FWM images. *J Raman Spectrosc* 40:941–7.
- Arora R, Petrov GI, Yakovlev VV, Scully MO. 2012. Detecting anthrax in the mail by coherent Raman microspectroscopy. *Proc Natl Acad Sci* 109:1151–3.
- Bar-Ilan O, Chuang CC, Schwahn DJ, Yang S, Joshi S, Pedersen JA, et al. 2013. TiO<sub>2</sub> Nanoparticle exposure and illumination during zebrafish development: mortality at parts per billion concentrations. *Environ Sci Technol* 47:4726–33.
- Belsey NA, Garrett NL, Contreras-Rojas LR, Pickup-Gerlaugh AJ, Price GJ, Moger J, et al. 2014. Evaluation of drug delivery to intact and porated skin by coherent Raman scattering and fluorescence microscopies. *J Control Release* 174:37–42.
- Blais DR, Lyn RK, Joyce MA, Rouleau Y, Steenbergen R, Barsby N, et al. 2010. Activity-based protein profiling identifies a host enzyme, carboxylesterase 1, which is differentially active during hepatitis C virus replication. *J Biol Chem* 285:25602–12.
- Caldorera-Moore M, Guimard N, Shi L, Roy K. 2010. Designer nanoparticles: incorporating size, shape and triggered release into nanoscale drug carriers. *Expert Opin Drug Deliv* 7:479–95.
- Cheng C, Porter AE, Muller K, Koziol K, Skepper JN, Midgley P, Welland M. 2009a. Imaging carbon nanoparticles and related cytotoxicity. *J Phys: Conf Ser* 151:012030.
- Cheng J, Flahaut E, Cheng SH. 2007. Effect of carbon nanotubes on developing zebrafish (*Danio rerio*) embryos. *Environ Toxicol Chem* 26:708–16.
- Cheng JP, Chan CM, Veca LM, Poon WL, Chan PK, Qu LW, et al. 2009b. Acute and long-term effects after single loading of functionalized multi-walled carbon nanotubes into zebrafish (*Danio rerio*). *Toxicol Appl Pharmacol* 235:216–25.
- Cheng JX, Jia YK, Zheng GF, Xie XS. 2002b. Laser-scanning coherent anti-Stokes Raman scattering microscopy and applications to cell biology. *Biophys J* 83:502–9.
- Cheng JX, Volkmer A, Book LD, Xie XS. 2001. An epi-detected coherent anti-Stokes raman scattering (E-CARS) microscope with high spectral resolution and high sensitivity. *J Phys Chem B* 105:1277–80.
- Cheng JX, Volkmer A, Xie XS. 2002a. Theoretical and experimental characterization of coherent anti-Stokes Raman scattering microscopy. *J Opt Soc Am B* 19:1363–75.
- Cole M, Lindeque P, Fileman E, Halsband C, Goodhead R, Moger J, et al. 2013. Microplastic ingestion by zooplankton. *Environ Sci Technol* 47:6646–55.
- Evans CL, Xie XS. 2008. Coherent anti-Stokes Raman scattering microscopy: chemical imaging for biology and medicine. *Annu Rev Anal Chem* 1:883–909.
- Fabrega J, Tantra R, Amer A, Stolpe B, Tomkins J, Fry T, et al. 2011. Sequestration of zinc from zinc oxide nanoparticles and life cycle effects in the sediment dweller amphipod *Corophium volutator*. *Environ Sci Technol* 46:1128–35.
- Fan Q-L, Neoh K-G, Kang E-T, Shuter B, Wang S-C. 2007. Solvent-free atom transfer radical polymerization for the preparation of poly(poly(ethyleneglycol) monomethacrylate)-grafted Fe<sub>3</sub>O<sub>4</sub> nanoparticles: synthesis, characterization and cellular uptake. *Biomaterials* 28:5426–36.
- Ferry JL, Craig P, Hexel C, Sisco P, Frey R, Pennington PL, et al. 2009. Transfer of gold nanoparticles from the water column to the estuarine food web. *Nat Nano* 4:441–4.
- Freudiger CW, Min W, Saar BG, Lu S, Holtom GR, He C, et al. 2008. Label-free biomedical imaging with high sensitivity by stimulated Raman scattering microscopy. *Science* 322:1857–61.
- Galloway T, Lewis C, Dolciotti I, Johnston BD, Moger J, Regoli F. 2010. Sublethal toxicity of nano-titanium dioxide and carbon nanotubes in a sediment dwelling marine polychaete. *Environ Pollut* 158:1748–55.
- Garrett N, Whiteman M, Moger J. 2011. Imaging the uptake of gold nanoshells in live cells using plasmon resonance enhanced four wave mixing microscopy. *Opt Express* 19:17563–74.
- Gonda K, Watanabe TM, Ohuchi N, Higuchi H. 2010. *In vivo* nano-imaging of membrane dynamics in metastatic tumor cells using quantum dots. *J Biol Chem* 285:2750–7.
- Grieger KD, Baun A, Owen R. 2010. Redefining risk research priorities for nanomaterials. *J Nanopart Res* 12:383–92.
- Hashimoto M, Araki T, Kawata S. 2000. Molecular vibration imaging in the fingerprint region by use of coherent anti-Stokes Raman scattering microscopy with a collinear configuration. *Opt Lett* 25:1768–70.
- Hellerer T, Axäng C, Brackmann C, Hillertz P, Pilon M, Enejder A. 2007. Monitoring of lipid storage in *Caenorhabditis elegans* using coherent anti-Stokes Raman scattering (CARS) microscopy. *Proc Natl Acad Sci* 104:14658–63.
- Helmchen F, Denk W. 2005. Deep tissue two-photon microscopy. *Nat Methods* 2:932–40.
- Hendry E, Hale PJ, Moger J, Savchenko AK, Mikhailov SA. 2010. Coherent nonlinear optical response of graphene. *Phys Rev Lett* 105:097401.
- Ichimura T, Hayazawa N, Hashimoto M, Inouye Y, Kawata S. 2004. Tip-enhanced coherent anti-Stokes Raman scattering for vibrational nanoimaging. *Phys Rev Lett* 92:220801.
- Jain RK, Lind RC. 1983. Degenerate four-wave mixing in semiconductor-doped glasses. *J Opt Soc Am* 73:647–53.
- Jia NQ, Lian Q, Tian Z, Duan X, Yin M, Jing LH, et al. 2010. Decorating multi-walled carbon nanotubes with quantum dots for construction of multi-colour fluorescent nanoprobes. *Nanotechnology* 21:045606.
- Johnston BD, Scown TM, Moger J, Cumberland SA, Baalousha M, Linge K, et al. 2010a. Bioavailability of nanoscale metal oxides TiO<sub>2</sub>, CeO<sub>2</sub> and ZnO to Fish. *Environ Sci Technol* 44:1144–51.
- Johnston HJ, Semmler-Behnke M, Brown DM, Kreyling W, Tran L, Stone V. 2010b. Evaluating the uptake and intracellular fate of polystyrene nanoparticles by primary and hepatocyte cell lines *in vitro*. *Toxicol Appl Pharmacol* 242:66–78.
- Jung Y, Chen H, Tong L, Cheng J-X. 2009. Imaging gold nanorods by plasmon-resonance-enhanced four wave mixing. *J Phys Chem C* 113:2657–63.
- Kahru A, Doubourguier H-C. 2010. From ecotoxicology to nanoeotoxicology. *Toxicology* 269:105–19.
- Kim H, Sheps T, Collins PG, Potma EO. 2009. Nonlinear optical imaging of individual carbon nanotubes with four-wave-mixing microscopy. *Nano Lett* 9:2991–5.
- Lalatsa A, Garrett NL, Ferrarelli T, Moger J, Schätzlein AG, Uchegbu IF. 2012. Delivery of peptides to the blood and brain after oral uptake of quaternary ammonium palmitoyl glycol chitosan nanoparticles. *Mol Pharm* 9:1764–74.
- Lam CW, James JT, McCluskey R, Arepalli S, Hunter RL. 2006. A review of carbon nanotube toxicity and assessment of potential occupational and environmental health risks. *Crit Rev Toxicol* 36:189–217.
- Larner F, Dogra Y, Dybowska A, Fabrega J, Stolpe B, Bridgestock LJ, et al. 2012. Tracing bioavailability of ZnO nanoparticles using stable isotope labeling. *Environ Sci Technol* 46:12137–45.
- Lee KJ, Nallathamby PD, Browning LM, Osgood CJ, Xu X-HN. 2007. *In vivo* imaging of transport and biocompatibility of single silver nanoparticles in early development of zebrafish embryos. *ACS Nano* 1:133–43.
- Lefrant S, Buisson J-P, Mevellec J-Y, Baltog I, Baibarac M. 2008. Single-beam pumped coherent anti-Stokes Raman scattering on carbon nanotubes. *Phys Status Solidi B* 245:2221–4.
- Lu K, Zhang ZY, He XA, Ma YH, Zhou KB, Zhang HF, et al. 2010. Bioavailability and distribution and of ceria nanoparticles in simulated aquatic ecosystems, quantification with a radiotracer technique. *J Nanosci Nanotechnol* 10:8658–62.
- Maker PD, Terhune RW. 1965. Study of optical effects due to an induced polarisation third order in electric field strength. *Phys Rev* 137:A801–18.
- Mansfield JC, Littlejohn GR, Seymour MP, Lind RJ, Perfect S, Moger J. 2013. Label-free chemically specific imaging in planta with stimulated Raman scattering microscopy. *Anal Chem* 85:5055–63.
- Menard A, Drobne D, Jemec A. 2011. Ecotoxicity of nanosized TiO<sub>2</sub>. Review of *in vivo* data. *Environ Pollut* 159:677–84.
- Moger J, Johnston BD, Tyler CR. 2008. Imaging metal oxide nanoparticles in biological structures with CARS microscopy. *Opt Express* 16:3408–19.
- Mouchet F, Landois P, Sarremejean E, Bernard G, Puech P, Pinelli E, et al. 2008. Characterisation and *in vivo* ecotoxicity evaluation of

- double-wall carbon nanotubes in larvae of the amphibian *Xenopus laevis*. *Aquat Toxicol* 87:127–37.
- Murphy CJ, Gole AM, Stone JW, Sisco PN, Alkilany AM, Goldsmith EC, et al. 2008. Gold nanoparticles in biology: beyond toxicity to cellular imaging. *Accounts Chem Res* 41:1721–30.
- Nan X, Tonary AM, Stolow A, Xie XS, Pezacki JP. 2006. Intracellular imaging of HCV RNA and cellular lipids by using simultaneous two-photon fluorescence and coherent anti-Stokes Raman scattering microscopies. *ChemBioChem* 7:1895–7.
- Oberdorster G. 2010. Safety assessment for nanotechnology and nanomedicine: concepts of nanotoxicology. *J Intern Med* 267: 89–105.
- Osborne OJ, Johnston BD, Moger J, Balousha M, Lead JR, Kudoh T, et al. 2013. Effects of particle size and coating on nanoscale Ag and TiO<sub>2</sub> exposure in zebrafish (*Danio rerio*) embryos. *Nanotoxicology* 7: 1315–24.
- Park J-H, Gu L, von Maltzahn G, Ruoslahti E, Bhatia SN, Sailor MJ. 2009. Biodegradable luminescent porous silicon nanoparticles for *in vivo* applications. *Nat Mater* 8:331–6.
- Petri-Fink A, Steitz B, Finka A, Salaklang J, Hofmann H. 2008. Effect of cell media on polymer coated superparamagnetic iron oxide nanoparticles (SPIONs): colloidal stability, cytotoxicity and cellular uptake studies. *Eur J Pharm Biopharm* 68:129–37.
- Pope I, Payne L, Zorinants G, Thomas E, Williams O, Watson P, et al. 2014. Coherent anti-Stokes Raman scattering microscopy of single nanodiamonds. *Nat Nanotechnol* 9:940–6.
- Porter AE, Gass M, Muller K, Skepper JN, Midgley P, Welland M. 2007a. Visualizing the uptake of C-60 to the cytoplasm and nucleus of human monocyte-derived macrophage cells using energy-filtered transmission electron microscopy and electron tomography. *Environ Sci Technol* 41: 3012–17.
- Porter AE, Gass M, Muller K, Skepper JN, Midgley PA, Welland M. 2007b. Direct imaging of single-walled carbon nanotubes in cells. *Nat Nanotechnol* 2:713–17.
- Ribeiro F, Gallego-Urrea JA, Goodhead RM, Van Gestel CAM, Moger J, Soares AMVM, Loureiro S. 2014. Uptake and elimination kinetics of silver nanoparticles and silver nitrate by *Raphidocelis subcapitata*: the influence of silver behavior in solution. *Nanotoxicology*. [Epub ahead of print]. doi: 10.3109/17435390.2014.963724.
- Rodriguez LG, Lockett SJ, Holtom GR. 2006. Coherent anti-stokes Raman scattering microscopy: a biological review. *Cytometry A* 69A: 779–91.
- Roh JY, Sim SJ, Yi J, Park K, Chung KH, Ryu DY, et al. 2009. Ecotoxicity of silver nanoparticles on the soil nematode *Caenorhabditis elegans* using functional ecotoxicogenomics. *Environ Sci Technol* 43: 3933–40.
- Schrand AM, Rahman MF, Hussain SM, Schlager JJ, Smith DA, Syed AF. 2010. Metal-based nanoparticles and their toxicity assessment. *Wiley Interdiscip Rev Nanomed Nanobiotechnol* 2:544–68.
- Scown TM, Goodhead RM, Johnston BD, Moger J, Baalousha M, Lead JR, et al. 2010. Assessment of cultured fish hepatocytes for studying cellular uptake and (eco)toxicity of nanoparticles. *Environ Chem* 7:36–49.
- Scown TM, van Aerle R, Johnston BD, Cumberland S, Lead JR, Owen R, et al. 2009. High doses of intravenously administered titanium dioxide nanoparticles accumulate in the kidneys of rainbow trout but with no observable impairment of renal function. *Toxicol Sci* 109:372–80.
- Soto KF, Carrasco A, Powell TG, Garza KM, Murr LE. 2005. Comparative *in vitro* cytotoxicity of some manufactured nanoparticulate materials characterised by transmission electron microscopy. *J Nanopart Res* 7:145–69.
- Sumner SCJ, Fennell TR, Snyder RW, Taylor GF, Lewin AH. 2010. Distribution of carbon-14 labeled C60 ([<sup>14</sup>C]C60) in the pregnant and in the lactating dam and the effect of C60 exposure on the biochemical profile of urine. *J Appl Toxicol* 30:354–60.
- Svoboda K, Block SM. Biological applications of optical forces. *Annu Rev Biophys Biomol Struct* 1994;23:247–285.
- Tantra R, Cumpson P. 2007. The detection of airborne carbon nanotubes in relation to toxicology and workplace safety. *Nanotoxicology* 1: 251–65.
- Tantra R, Knight A. 2011. Cellular uptake and intracellular fate of engineered nanoparticles: a review on the application of imaging techniques. *Nanotoxicology* 5:381–92.
- Tong L, Lu Y, Lee RJ, Cheng J-X. 2007. Imaging receptor-mediated endocytosis with a polymeric nanoparticle-based coherent anti-Stokes Raman scattering probe. *J Phys Chem B* 111:9980–5.
- Volkmer A, Cheng JX, Xie XS. 2001. Vibrational imaging with high sensitivity via epidetected coherent anti-Stokes Raman scattering microscopy. *Phys Rev Lett* 87:023901.
- Wang Y, Lin C-Y, Nikolaenko A, Raghunathan V, Potma EO. 2011. Four-wave mixing microscopy of nanostructures. *Adv Opt Photon* 3: 1–52.
- Watts AJR, Lewis C, Goodhead RM, Beckett SJ, Moger J, Tyler CR, Galloway TS. 2014. Uptake and retention of microplastics by the shore crab *Carcinus maenas*. *Environ Sci Technol* 48:8823–30.
- Wynne JJ. 1969. Optical third-order mixing in GaAs, Ge, Si and InAs. *Phys Rev* 178:1295–303.
- Xu P, Gullotti E, Tong L, Highley CB, Errabelli DR, Hasan T, et al. 2008. Intracellular drug delivery by poly(lactic-co-glycolic acid) nanoparticles, revisited. *Mol Pharm* 6:190–201.
- Zumbusch A, Holtom GR, Xie XS. 1999. Three-dimensional vibrational imaging by coherent anti-Stokes Raman scattering. *Phys Rev Lett* 82: 4142–5.

Supplementary material available online  
Supplementary Videos